Cohesive Zone Criterion for Cracking along the Cu/Si Interface in Nanoscale Components

Yabin Yan [a,*], Takashi Sumigawa [a], Fulin Shang [b], Takayuki Kitamura [a]

[a] *Department of Mechanical Engineering and Science, Kyoto University, Kyoto 606-8501, Japan*

[b] *Department of Engineering Mechanics, Xi'an Jiaotong University, Xi'an 710049, China*

Abstract

Crack initiation and propagation along the Cu/Si interface in multilayered films (Si/Cu/SiN) with different thicknesses of the Cu layer (20 and 200 nm) are experimentally investigated using a nano-cantilever and millimeter-sized four-point bending specimens. To examine the cohesive zone model (CZM) criterion for interfacial delamination along the Cu/Si interface in nanoscale stress concentration, an exponential type of CZM is utilized to simulate the observed delamination processes using the finite element method. After the CZM parameters for the Cu/Si interface are calibrated by experiment, interface cracking in other experiments is predicted. This indicates that the CZM criterion is universally applicable for describing cracking along the interface regardless of specimen dimensions and film thickness which include the differences in plastic behavior and residual stress. The CZM criterion can also predict interfacial cracking along Cu/Si interfaces with different stress singularities.

Keywords: Interface; Cohesive zone model; Nano-component; Delamination; Nanoscale; Crack initiation; Crack propagation; Interface crack; Thin film; Plasticity; Residual stress

---

* Corresponding author. Tel: +81 75 753 5192; fax: +81 75 753 5256.
E-mail address: yan.yabin@ht5.ecs.kyoto-u.ac.jp (Y. Yan).

1. Introduction

Many advanced microelectronic and micromechanical devices consist of dissimilar materials, and intrinsic bi-material interfaces are inevitably introduced into these devices. Such an interface is a potential site for cracking due to stress concentration originating from deformation mismatch. Thus, in order to assure reliability of the devices, it is critically important to correctly evaluate the interface strength under nanoscale stress concentration.

Fracture mechanics theory has been widely used to investigate interfacial delamination in bulk materials [1-4] and the stress intensity factor or energy release rate characterizes the fracture toughness of the bi-material interface. Recently, experimental and analytical studies have also been conducted on interfacial delamination in nanoscale components [5-7]. Crack initiation from the interface edge, for example, was investigated using a nano-cantilever method [8-11], while crack propagation along an interface in multilayered films was examined using a four-point bending specimen [8, 12-15]. The applicability of fracture mechanics was discussed on the basis of respective stress intensity factors.

However, to universally describe the interface toughness, this approach clearly has disadvantages. Since the stress field at the crack tip possesses much higher singularity than at the interface free edge, the corresponding stress intensity factors have different dimensions. Moreover, plastic deformation and residual stress influence the singular field. Therefore, it is necessary to find an appropriate approach to evaluate the fracture toughness of interfaces.

As a phenomenological model within the framework of continuum mechanics, the cohesive zone model (CZM) for cracking in bulk components has attracted considerable

attention, as it represents a powerful and efficient tool to simulate fracture toughness of the interface. The application of CZMs to bi-material interfacial delamination has been successful in many material systems [16-19]. Primary conceptual work on CZM was carried out by Barenblatt [20], who proposed CZM to study brittle materials, and Dugdale [21], who adopted a fracture process zone concept to investigate ductile materials exhibiting plasticity. During the past decades, many types of constitutive equations, or traction-separation laws, were used in CZMs, including those of polynomial type [22, 23], trapezoid type [24], bilinear type [25], and exponential type [26]. However, until now, the application of CZM has mainly focused on interfacial delamination in macroscopic materials except for a few studies [27, 28]. Application for delamination induced by nanoscale stress concentration in small components has not been fully investigated. Thus, it is necessary to examine the applicability of CZM for fracture problems in nano-components.

In this study, a CZM of exponential type [26] is used to simulate the observed crack initiation at the Cu/Si interface edge and propagation along the Cu/Si interface with nanoscale stress concentration in different experiments [8, 9]. We examine the reliability of the CZM fracture concept for nanoscale components on the basis of experiments and analyses.

2. Experiments on initiation and propagation of interface crack

2.1 Materials tested

The tested materials are multilayer Si/Cu/Si_3N_4 (silicon/copper/silicon nitride) with different Cu thicknesses. After a Si (100) wafer surface is cleaned by inverse sputtering, a Cu layer with a thickness of 20 or 200 nm is deposited by radio-frequency (RF)

magnetron sputtering in a 0.67 Pa Argon atmosphere. A Si_3N_4 (abbreviated as SiN in following) thin layer of about 500 nm thickness is then formed on the Cu layer.

Since the yield stress of the Cu layer is much lower than that of the Si substrate ($\sigma_{y,Si}$ > 3.4 GPa [29]) and the SiN layer ($\sigma_{y,SiN}$ > 8.4 GPa [30]), only the Cu layer should be subject to elasto-plastic deformation during experiments. By using the Von Mises equivalent stress σ and strain ε, the elasto-plastic behaviors of 20 nm [10] and 200 nm thick [11] Cu layers are experimentally investigated and the constitutive relation is given as follows:

$$\sigma = \begin{cases} E\varepsilon, & \sigma \le \sigma_y \\ R\varepsilon^n, & \sigma \ge \sigma_y \end{cases} \tag{1}$$

where σ_y, R, n, E are the yield stress, strength coefficient, strain hardening exponent, and Young's modulus, respectively, and their magnitudes for the 20 and 200 nm-thick Cu layers are listed in Table 1. It should be noted that the plastic behavior of a thin film often shows eminent size-dependence.

In addition, the residual stresses introduced during the processing are examined experimentally [10] and are listed in Table 1 as well.

Table 1 Constitutive constants and residual stresses of 20 and 200 nm-thick Cu layers

Thickness of Cu layer, nm	σ_y, MPa	R, MPa	n	E, GPa	Residual stress in Cu layer, MPa	Residual stress in SiN layer, MPa
20	765	3316	0.3	129	760	-290
200	345	2049	0.3	129	147	-483

2.2 Nano-cantilever experiment [8, 9]

2.2.1 Specimens and experimental set-ups

In this experiment, the nano-cantilever method [8, 9] is adopted to investigate crack initiation at the Cu/Si interface edge in the multilayered thin film. Fig. 1 shows a schematic illustration of the nano-cantilever specimen used for the delamination experiments of the Cu thin films with thicknesses of 20 and 200 nm. These are denoted as "nano-cantilever (20 nm Cu)" and " nano-cantilever (200 nm Cu)", respectively. The study focus is on crack initiation at the Cu/Si interface edge. A protective layer (gold for the material with 20 nm-thick Cu, platinum and carbon for the material with 200 nm-thick Cu) is deposited on the SiN layer to prevent specimen damage during specimen preparation by focused ion beam (FIB) technology. Several experiments are carried out for each material to examine experimental reliability.

A minute mechanical loading apparatus (Nanofactory Instruments AB, SA2000N) is used to apply a force and the behavior of interface fracture is observed *in situ* by transmission electron microscopy (TEM). The load is applied to the SiN layer by pushing the specimen against a diamond loading tip at the velocity of 8 nm/s, and then the Cu/Si interface is stressed by a bending moment, as illustrated in Fig. 1. TEM observations confirmed that no damage or defect is present on the Cu/Si interface edge before the experiments.

Specimen No.	w_{Cu}	w_{Si}	w_{SiN}	w_{Prot}	d	h	ϕ_{Si}/ϕ_{Cu},°

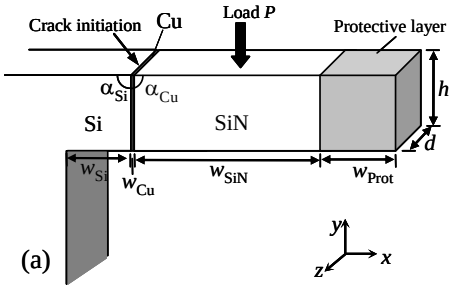

Specimen No.	w_{Cu}	w_{Si}	w_{SiN}	w_{Prot}	d	h	ϕ_{Si}/ϕ_{Cu},°
Nano-cantilever (20 nm Cu)-A1	20	220	480	235	250	434	90/90
Nano-cantilever (20 nm Cu)-A2	20	120	480	220	308	233	90/90
Nano-cantilever (20 nm Cu)-A3	20	84	480	287	415	642	90/90

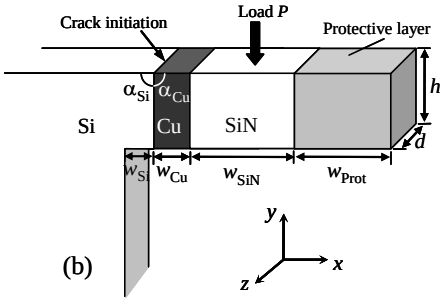

Specimen No.	w_{Cu}	w_{Si}	w_{SiN}	w_{Prot}	d	h	ϕ_{Si}/ϕ_{Cu},°
Nano-cantilever (200 nm Cu)-I1	200	110	470	490	340	300	87/93
Nano-cantilever (200 nm Cu)-I2	200	205	400	490	260	320	77/103
Nano-cantilever (200 nm Cu)-I3	200	100	470	490	390	290	90/90
Nano-cantilever (200 nm Cu)-I4	200	82	480	-	320	980	78/102

Fig. 1 Schematic illustration of specimens with (a) 20 nm-thick Cu thin film (nano-cantilever (20 nm Cu)) and (b) 200 nm-thick Cu thin film (nano-cantilever (200 nm Cu)). The length scale is in nanometers

2.2.2 Experimental results

Fig. 2 shows the relationships between the applied load and deflection at the end of the cantilever arm under monotonic loading of nano-cantilever (200 nm Cu) tests, where the deflection is quantitatively measured from the TEM images. For comparison, the fully elastic load-deflection curve obtained by FEM calculation (dashed lines) of each nano-cantilever (200 nm Cu) specimen is also shown in Fig. 2. At a low load level, the relationship is linear, which suggests fully elastic deformation. With an increase in the applied load, the experimental curves become nonlinear by plastic deformation in the

Cu layer [11]. At the critical load, the crack initiates at the edge of the Cu/Si interface, and subsequently leads to complete delamination of the entire interface. The experimental curves possess different stiffness due to the difference in specimen size. Similar fracture behavior is observed in the nano-cantilever (20 nm Cu) experiments [10]. Fig. 3 shows the TEM micrographs of specimen A1 of nano-cantilever (20 nm Cu) tests (a) before applying load, (b) under the critical load, and (c) after the crack initiation. The critical load, P_C, for crack initiation is listed in Table 2, which shows that it is greatly dependent on the specimen geometry.

It should be noted that the stress-concentrated area is confined to the tens of nanometers scale, as shown later in section 7 (see Fig. 11).

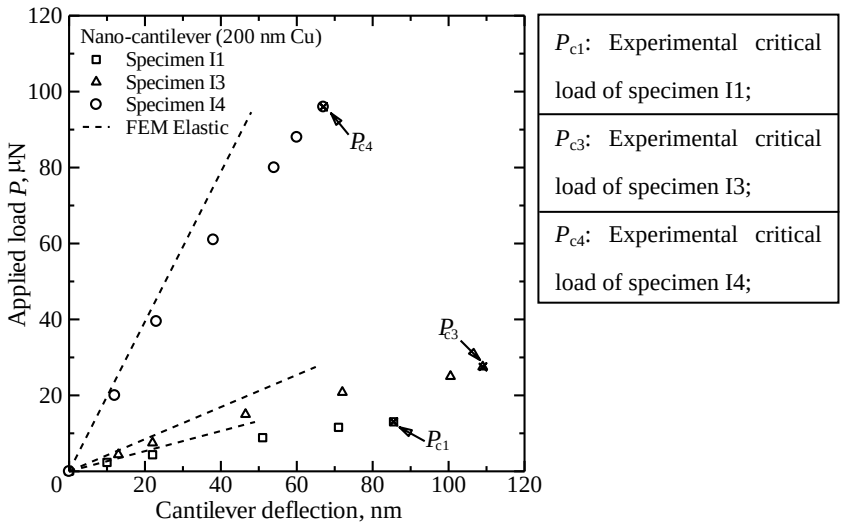

Fig. 2 Relationship between applied load and cantilever deflection for specimens I1, I3, and I4 of the nano-cantilever (200 nm Cu) tests. Dashed lines are curves obtained by fully elastic FEM calculations

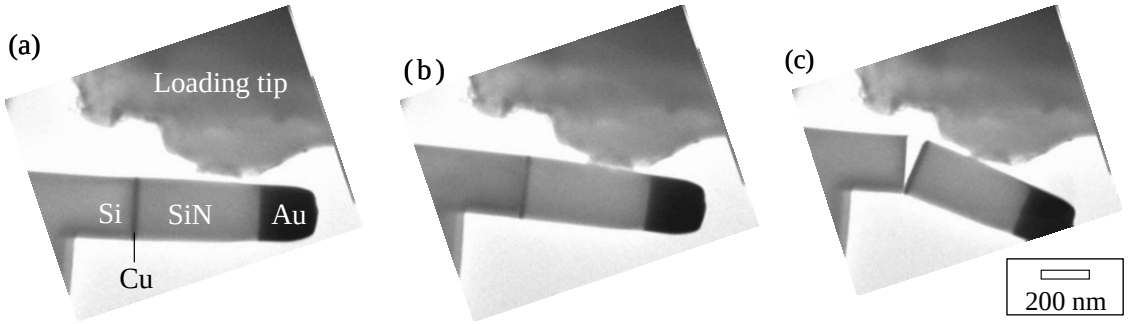

Fig.3 TEM micrographs of specimen A1 of nano-cantilever (20 nm Cu) tests. (a) before applying load; (b) under the critical load; (c) after crack initiation

Table 2 Critical loads, P_C, of the nano-cantilever specimens

Specimen No.	Critical load, P_C, μN
Nano-cantilever (20 nm Cu)-A1	16.9
Nano-cantilever (20 nm Cu)-A2	10.3
Nano-cantilever (20 nm Cu)-A3	85.3
Nano-cantilever (200 nm Cu)-I1	13.0
Nano-cantilever (200 nm Cu)-I2	11.7
Nano-cantilever (200 nm Cu)-I3	27.5
Nano-cantilever (200 nm Cu)-I4	94.6

2.3 Modified four-point bending experiment [8]

2.3.1 Specimens and experimental set-ups

In order to investigate the crack propagation along the Cu/Si interface, a modified four-point bending method [8] is adopted. A rectangular coupon with millimeter-scale width and length is cut from the material with the 200 nm-thick Cu thin film. A plate of stainless steel is glued to the coupon using epoxy, as schematically shown in Fig. 4. It should be noted that the whole specimen size is millimeter-scale, which is almost a thousand times larger than those of the nano-cantilever specimens shown in Fig. 1. The experiment focus in this case is on the criterion of crack propagation along the Cu/Si interface from the pre-existing crack. Three specimens are tested to assure reliability of

the experimental results.

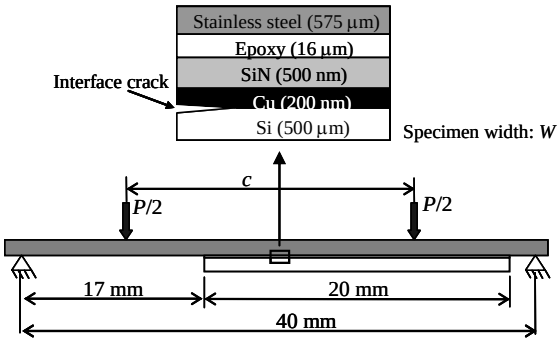

Specimen No.	width, *W*, mm
Four-point bending (200 nm Cu)-P1	5.58
Four-point bending (200 nm Cu)-P2	4.79
Four-point bending (200 nm Cu)-P3	4.54

Fig. 4 Schematic of the modified four-point bending specimen (200 nm Cu) and the loading system

2.3.2 Experimental results

After an interfacial pre-crack is introduced into the specimen by using a short span between the inner loading points c (c = 10 mm is used here), the crack propagation experiments are conducted at c = 18 mm. The load P is applied to it by a testing machine with an electro-magnetic actuator (Shimadzu, MMT-100N) at a constant displacement rate of 1 μm/s. Table 3 shows the critical load, P_C, for crack propagation in all the tested specimens. The obtained critical loads are nearly a million times larger than those in the nano-cantilever tests (Table 2) due to the huge difference in the specimen dimensions. However, the stress-concentrated area is confined to the tens of nanometers scale, as discussed in section 7 (Fig. 11).

Table 3 Critical loads, P_C, of the modified four-point bending specimens

Specimen No.	Critical load P_C, μN
Four-point bending (200 nm Cu)-P1	5.40×10^6
Four-point bending (200 nm Cu)-P2	4.86×10^6
Four-point bending (200 nm Cu)-P3	4.65×10^6

3. Cohesive zone model

In most CZMs, with increasing interfacial separation, the tractions across the interface increase to reach a maximum, and then decrease, eventually vanishing with complete decohesion. In this study, a CZM of exponential type [26] is adopted, which is one of the most popular cohesive zone laws. This exponential CM has some advantages for implementation. For example, the tractions and their derivatives in the exponential CZM are continuous, which improves the convergence of the numerical simulation process for interface cracking. The constitutive relation of exponential CZM is briefly described below.

In the exponential CZM, the interfacial potential is defined as

$$\phi(\Delta_{\mathrm{n}},\Delta_{\mathrm{t}})=\phi_{\mathrm{n}}+\phi_{\mathrm{n}}\exp(-\frac{\Delta_{\mathrm{n}}}{\delta_{\mathrm{n}}})\{[1-r+\frac{\Delta_{\mathrm{n}}}{\delta_{\mathrm{n}}}]\frac{1-q}{r-1}-[q+(\frac{r-q}{r-1})\frac{\Delta_{\mathrm{n}}}{\delta_{\mathrm{n}}}]\exp(-\frac{\Delta_{\mathrm{t}}^2}{\delta_{\mathrm{t}}^2})\} \tag{2}$$

with

$$q=\phi_{\mathrm{t}}/\phi_{\mathrm{n}}\text{ , and }\ r=\Delta_{\mathrm{n}}^{*}/\delta_{\mathrm{n}}\text{ ,} \tag{3}$$

where ϕ_{n} and ϕ_{t} are the work of the normal and shear separations, respectively; Δ_{n} and Δ_{t} are the normal and shear displacement jumps, respectively; δ_{n} and δ_{t} are the normal and shear interface characteristic length parameters. Δ_{n}^{*} is the magnitude of Δ_{n} at complete shear separation, where the normal traction is zero.

The relations between the interfacial tractions and the potential are given by

$$T_{\mathrm{n}}=\frac{\partial\phi}{\partial\Delta_{\mathrm{n}}},\text{ and }T_{\mathrm{t}}=\frac{\partial\phi}{\partial\Delta_{\mathrm{t}}}. \tag{4}$$

Substituting Eq. (2) into Eq. (4), we obtain the normal traction T_{n} and the shear traction T_{t} across the interface as follows

$$T_{\mathrm{n}}=(\frac{\phi_{\mathrm{n}}}{\delta_{\mathrm{n}}})\exp(-\frac{\Delta_{\mathrm{n}}}{\delta_{\mathrm{n}}})\{\frac{\Delta_{\mathrm{n}}}{\delta_{\mathrm{n}}}\exp(-\frac{\Delta_{\mathrm{t}}^2}{\delta_{\mathrm{t}}^2})+\frac{1-q}{r-1}[1-\exp(-\frac{\Delta_{\mathrm{t}}^2}{\delta_{\mathrm{t}}^2})](r-\frac{\Delta_{\mathrm{n}}}{\delta_{\mathrm{n}}})\} \tag{5}$$

$$T_{\mathrm{t}} = \frac{\phi_{\mathrm{n}}}{\delta_{\mathrm{n}}}\left(\frac{2\delta_{\mathrm{n}}}{\delta_{\mathrm{t}}}\right)\frac{\Delta_{\mathrm{t}}}{\delta_{\mathrm{t}}}\left(q + \frac{r-q}{r-1}\frac{\Delta_{\mathrm{n}}}{\delta_{\mathrm{n}}}\right)\exp\left(-\frac{\Delta_{\mathrm{n}}}{\delta_{\mathrm{n}}}\right)\exp\left(-\frac{\Delta_{\mathrm{t}}^2}{\delta_{\mathrm{t}}^2}\right) \tag{6}$$

With $\Delta_{\mathrm{t}} \equiv 0$, the normal traction-separation relation obtained from Eq. (5) is shown in Fig. 5(a), and Fig. 5(b) shows the variation of T_{t} with Δ_{t} given by Eq. (6) for $\Delta_{\mathrm{n}} \equiv 0$. The normal traction T_{n} reaches a peak value $\sigma_{\max}$ at an interface separation $\Delta_{\mathrm{n}} = \delta_{\mathrm{n}}$, and the shear traction T_{t} reaches a maximum value $\tau_{\max}$ at $|\Delta_{\mathrm{t}}| = \delta_{\mathrm{t}}/\sqrt{2}$, which gives

$$T_n\Big|_{\Delta_t \equiv 0, \Delta_n = \delta_n} = \sigma_{\max}, \quad T_t\Big|_{\Delta_n \equiv 0, \Delta_t = \delta_t/\sqrt{2}} = \tau_{\max} \tag{7}$$

Therefore, basing on Eqs. (3) and (5)~(7), the works of pure normal and pure shear separations, ϕ_{n} and ϕ_{t}, are related to $\sigma_{\max}$ and $\tau_{\max}$, respectively, by

$$\phi_{\mathrm{n}} = \sigma_{\max} e \delta_{\mathrm{n}}, \ \phi_{\mathrm{t}} = \sqrt{e/2}\,\tau_{\max}\delta_{\mathrm{t}} \tag{8}$$

where $e = \exp(1)$.

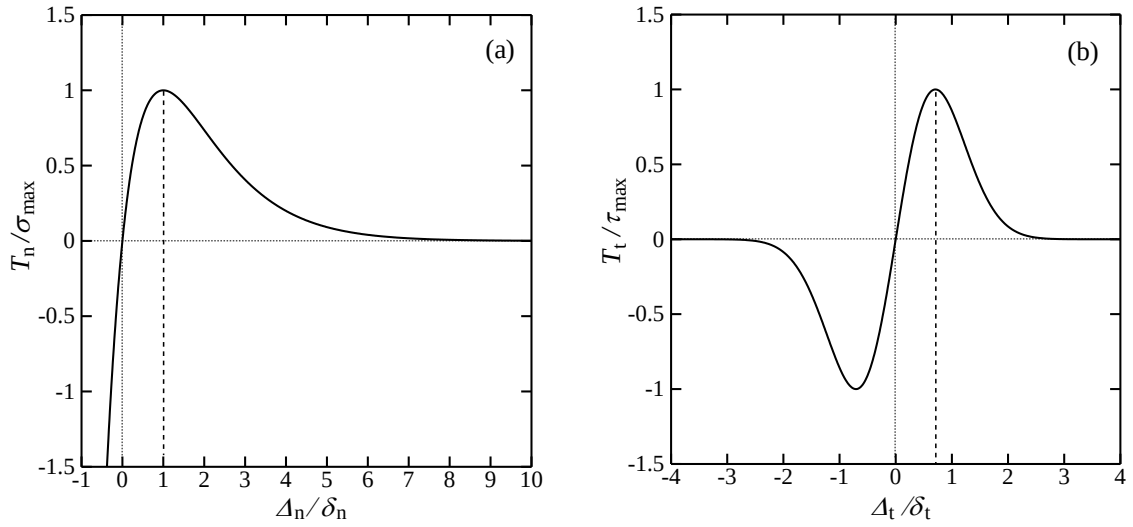

Fig. 5 (a) Normal traction, T_{n}, across the interface as a function of Δ_{n} with $\Delta_{\mathrm{t}} \equiv 0$. (b) Variation of shear traction, T_{t}, with Δ_{t} for $\Delta_{\mathrm{n}} \equiv 0$

4. Simulation method

Numerical simulation of the interfacial delamination is carried out using the finite element method (FEM) commercial software, ABAQUS. The Cu/Si interface is defined as a thin layer with zero thickness obeying the constitutive relation of the exponential

CZM, where the cohesive elements are arranged along the thin layer. The corresponding constitutive relation of CZM, *i.e.*, the traction-separation relation of the cohesive law, is implemented through the user subroutine UEL of ABAQUS. Corresponding plastic behaviors (Eq. (1) and Table 1) are respectively assigned to 20 and 200 nm-thick Cu layers, and corresponding residual stresses (Table 1) are imposed on the Cu layer and the SiN layer. For the other parts of the model, the properties listed in Table 4 are used for the analysis. Based on the geometric shape and loading condition, a plane strain state is assumed to simplify the simulations, and plane strain elements are used except on the interface. The area near the free edge of the interface or the pre-crack tip is carefully divided into fine meshes where the stress concentration or singularity is expected. Typical finite element meshes are shown in Fig. 6.

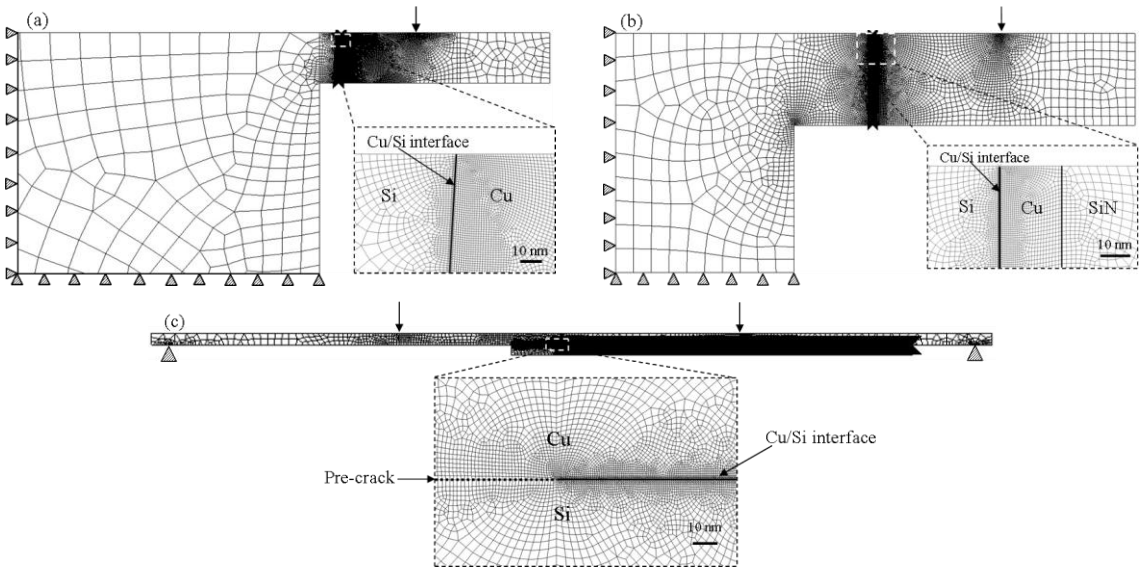

Fig. 6 Typical finite element meshes for numerical analysis: (a) nano-cantilever (200 nm Cu), (b) nano-cantilever (20 nm Cu), and (c) modified four-point bending (200 nm Cu) specimens

Table 4 Elastic constants of materials

Material	Young's modulus *E*, GPa	Poisson ratio, *v*
Cu	129	0.34
SiN	197	0.27
Si	130	0.28
Pt	171	0.39
C	400	0.30
Au	78	0.44
Epoxy	1.23	0.30
Stainless steel	200	0.30

5. Determination of CZM parameters

The CZM parameters are determined by calibrating the experimental results for specimen I1, which is one of the nano-cantilever (200 nm Cu) tests.

The independent parameters of CZM include the cohesive strength (σ_{max} and τ_{max}), and the interface characteristic length parameter (δ_n and δ_t), and the coupling parameter *r*. Since the normal stress is dominant on the interface near the edge and the crack tip in the delamination examined by the nano-cantilever and modified four-point bending specimens, the applicability of CZM for the mix mode delamination is beyond the scope of this paper. Thus, based on previous studies, the parameters *q* and *r* which represent the coupling behavior of mix mode fracture are set to unity and zero respectively, *i.e.*, $q=\phi_t/\phi_n=1$ and $r=\Delta_n^*/\delta_n=0$ [16, 31-34], and the normal and shear interface characteristic length parameters are assumed to have the same magnitude, *i.e.*, $\delta_{max}=\delta_n=\delta_t$ [16, 34-35]. We then have two independent parameters, σ_{max} and δ_{max}.

Trial-and-error calculations indicate that the cohesive strength, σ_{max}, is in the range of 900-1100 MPa for crack initiation at the interface edge. Thus, with σ_{max} = 1000 MPa, the effect of the interface characteristic length parameter, δ_{max}, is investigated using the

experimental data of specimen I1. As shown in Fig. 7, the slope of the calculated load-deflection curve is sensitive to the value of δ_{max}. With the decrease of δ_{max}, the slope of the calculated curve becomes steep. The simulation for δ_{max} = 1 nm results in the best correspondence with the slope of experimental curve. Then, the interface characteristic length parameter is set to 1 nm in subsequent calculations.

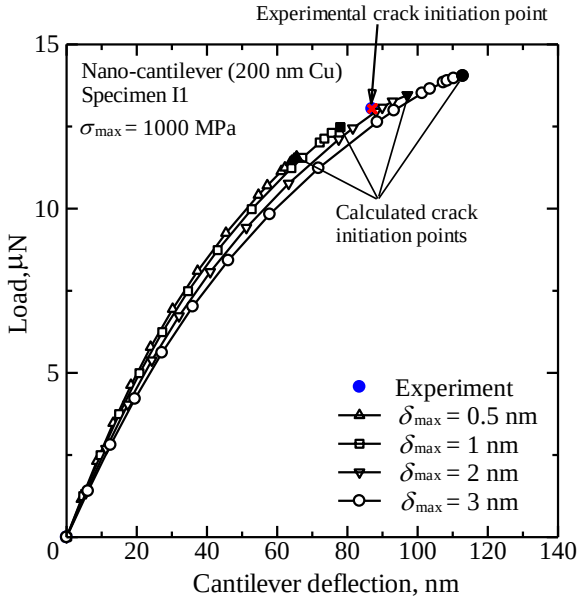

Fig. 7 Effect of interface characteristic length parameter, δ_{max}, on the calculated load-deflection curves

Fig. 8 shows the calculated load-deflection curves with different cohesive strengths under δ_{max} =1 nm, and Fig. 8(b) is an enlarged view of the square region in Fig. 8(a) near the critical load for the crack initiation. When the cohesive strength σ_{max} increases, the critical lateral forces become larger, while the slope of calculated curves remains constant. The simulation with σ_{max} = 1060 MPa gives good correspondence for the critical lateral force with the experimental results.

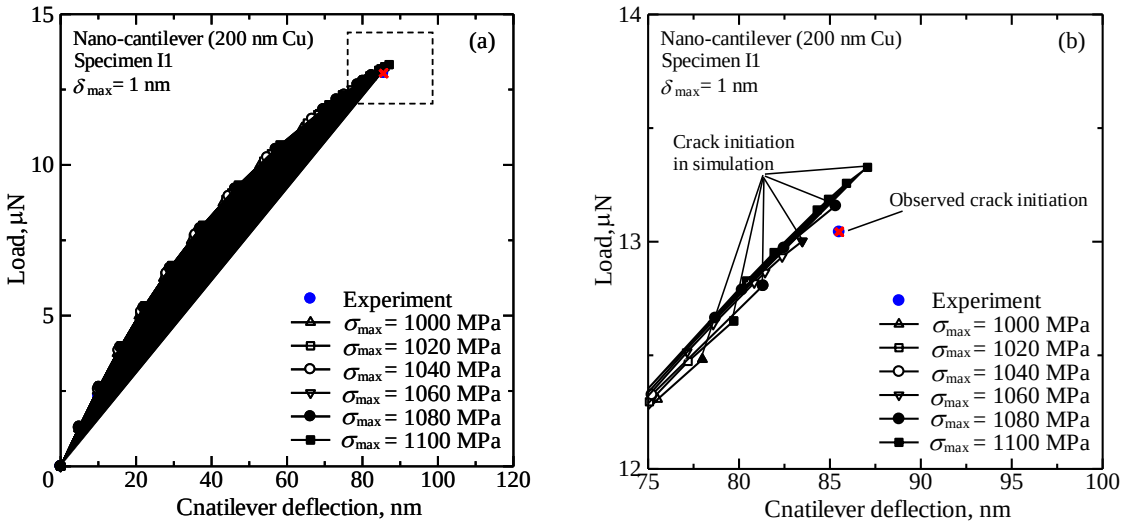

Fig. 8 Effect of the cohesive strength, σ_{max}, on the calculated critical loads for crack initiation

From the calibration, the CZM parameters of the Cu/Si interface are determined to be σ_{max} = 1060 MPa, and δ_{max} = 1 nm. Basing on Eq. (3) and Eq. (8), these give τ_{max} = 2472 MPa, and $\phi_n = \phi_t$ = 2.85 J/m^2.

6. Prediction of delamination based on the CZM parameters

6.1 Crack initiation in specimens with different sizes

The CZM parameters are determined solely from specimen I1. We explore the fundamental validity of the CZM by the other nano-cantilever (200 nm Cu) specimens, *i.e.*, I2, I3, and I4.

Table 5 shows the predicted critical loads for crack initiation obtained by the CZM analysis (σ_{max} = 1060 MPa, δ_{max} = 1 nm). Comparing with the experimental data, small relative errors between them implies that the CZM has the feasibility to prescribe the interface toughness for crack initiation at the Cu/Si interface edge. Since the difference in geometrical dimensions among the specimens is not large, especially the dimension

of the SiN layer which transfers the bending moment to the Cu/Si interface, this verification only reveals that the CZM can be regarded as a candidate method with universal applicability for predicting interface delamination in different specimens.

Table 5 Comparison of experimental and predicted critical loads for the nano-cantilever (200 nm Cu) tests

Specimen No.	Experimental P_c / μN	Calculated P_c' / μN	Relative error / %
Nano-cantilever (200 nm Cu)-I2	11.7	11.8	0.85
Nano-cantilever (200 nm Cu)-I3	27.5	26.2	4.72
Nano-cantilever (200 nm Cu)-I4	94.6	88.9	6.03

6.2 Crack initiation in specimens with Cu layer of different thickness (different plastic property and residual stress)

The thinner Cu layer possesses higher yield stress and stronger work hardening than the thicker Cu layer. In addition, the residual stress in the 20 nm-thick Cu layer is also different from that in the 200 nm-thick Cu layer. On the other hand, the interface structure must be same because the fabrication process for the Cu/Si interface is the same in both cases. Therefore, taking into account the plasticity and residual stress, the universal applicability of the CZM parameters for predicting crack initiation at the Cu/Si interface edge can be examined by the interface toughness of the nano-cantilevers (20 nm Cu) and (200 nm Cu).

Table 6 indicates the experimental and calculated critical loads of the nano-cantilever (20 nm Cu) at crack initiation under σ_{max} = 1060 MPa and δ_{max} = 1 nm. The good coincidence indicates that the CZM can generally represent the interface toughness for crack initiation at the Cu/Si interface with different plastic behavior, residual stress, and geometrical dimensions.

Table 6 Comparison of experimental and calculated critical loads for the nano-cantilever (20 nm Cu) tests

Specimen No.	Experimental P_c / μN	Calculated P_c' / μN	Relative error / %
Nano-cantilever (20 nm Cu)-A1	16.9	19.3	14.2
Nano-cantilever (20 nm Cu)-A2	10.3	10.7	3.88
Nano-cantilever (20 nm Cu)-A3	85.3	96.3	12.9

6.3 Crack propagation

The applicability to interface fracture in a strong singular field can be examined by predicting the crack propagation criterion obtained by the modified four-point bending experiment. Fig. 9 shows a comparison of the experimental and calculated load-displacement curves at the loading point. It can be seen that the CZM parameters determined with the nanoscale cantilever test can precisely predict the deformation behavior of the experiments on the millimeter level. In addition, Table 7 indicates the relative errors between the experimental and calculated critical loads for crack propagation. This shows that the CZM parameters can predict not only the crack initiation but also crack propagation along the Cu/Si interface. In other words, for predicting toughness under different singular fields, the CZM maintains its validity.

Table 7 Relative errors between experimental and calculated critical loads of modified four-point bending tests

Specimen No.	Experimental P_c / N	Calculated P_c' / N	Relative error /%
Four-point bending (200 nm Cu)-P1	5.40	5.11	5.37
Four-point bending (200 nm Cu)-P2	4.86	4.31	11.3
Four-point bending (200 nm Cu)-P3	4.65	4.18	10.1

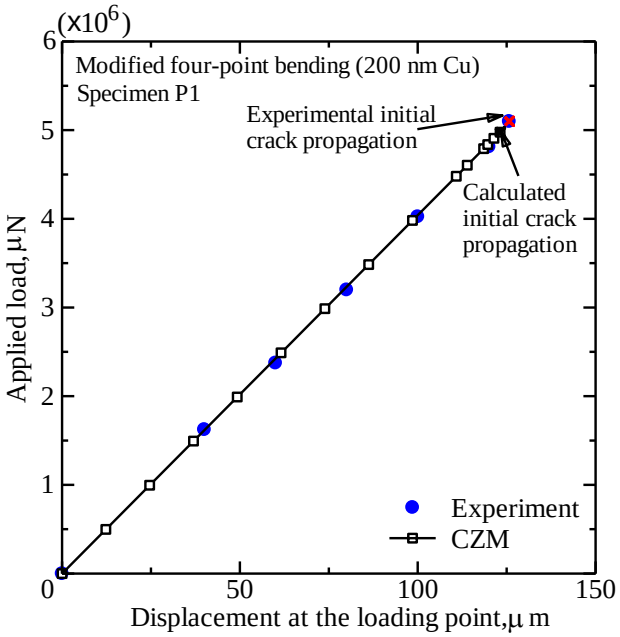

Fig. 9 Comparison of experimental and calculated load-displacement curves for specimen P1 of modified four-point bending (200 nm Cu) tests

6.4 Specimen size

The modified four-point bending specimens, P1-P3, have both the length and width on the millimeter scale, thousands of times larger than those of the nano-cantilever specimens, A1-A3 and I1-I4. Therefore, the independence of the CZM criterion on the geometrical size can be critically examined by the comparison.

All the experimental and predicted critical loads are compared in Fig. 10. The CZM parameters solely determined by specimen I1 can predict the toughness along the Cu/Si interface though the critical load magnitude has a difference of nearly 6 orders. This proves the versatility of the CZM criterion for the design of micro/nano devices.

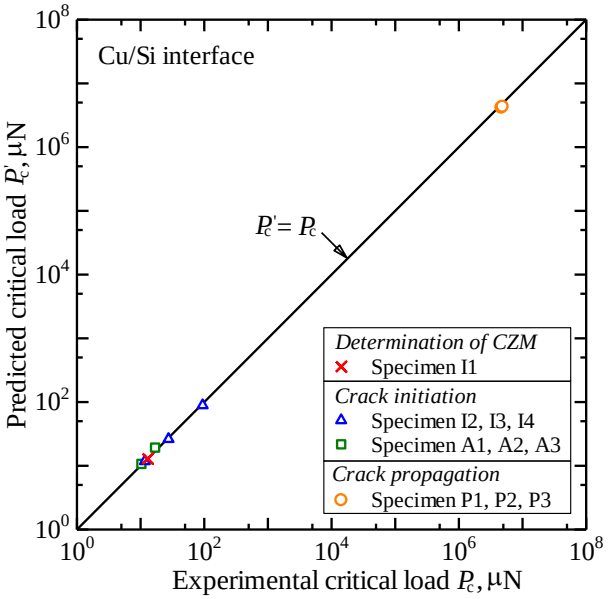

Fig. 10 Comparison of experimental and predicted critical loads of all tested specimens

7. Critical stress distribution along the Cu/Si interface

Fig. 11 shows the stress distributions along the Cu/Si interface with (solid lines; CZM) and without (dotted lines; n-CZM) the CZM for specimens A1 (nano-cantilever (20 nm Cu)), I1 (nano-cantilever (200 nm Cu)) and P1 (modified four-point bending (200 nm Cu)). The following discussion focuses on the distribution of the normal stress since it dominates the delamination process in these cases.

By arranging cohesive elements along the Cu/Si interface, the peak stress near the interface edge or crack tip is confined within the magnitude of the cohesive strength due to the degradation of cohesive elements. The CZM approximately brings about constant normal stress fields near the interface edge or crack tip, within a region 5 nm from the edge or crack tip. This suggests that this small region dominates the interfacial local fracture (crack initiation or propagation), *i.e.*, the fracture processing zone.

For specimen I1 and P1 of the 200 nm-thick Cu thin film, we notice that the singular stress zone is about 100 nm long. The length of the fracture processing zone (5

nm) is far smaller than that of the singular stress zone. This signifies that fracture mechanics theory is applicable in this material. However, it should be noticed that the dimensions of the stress intensity factor are different because the singular order is dependent on the shape of the interface edge or crack tip.

For specimen I1 and P1, there is little difference in the stress distribution in the simulations with and without the CZM except the fracture process zone. For specimen A1 from the 20 nm-thick Cu thin films, on the other hand, there is obvious deviation between the stress distributions with and without the CZM. This might indicate that conventional fracture mechanics is questionable for the specimen, though further experimental/analytical works are necessary for a more detailed understanding.

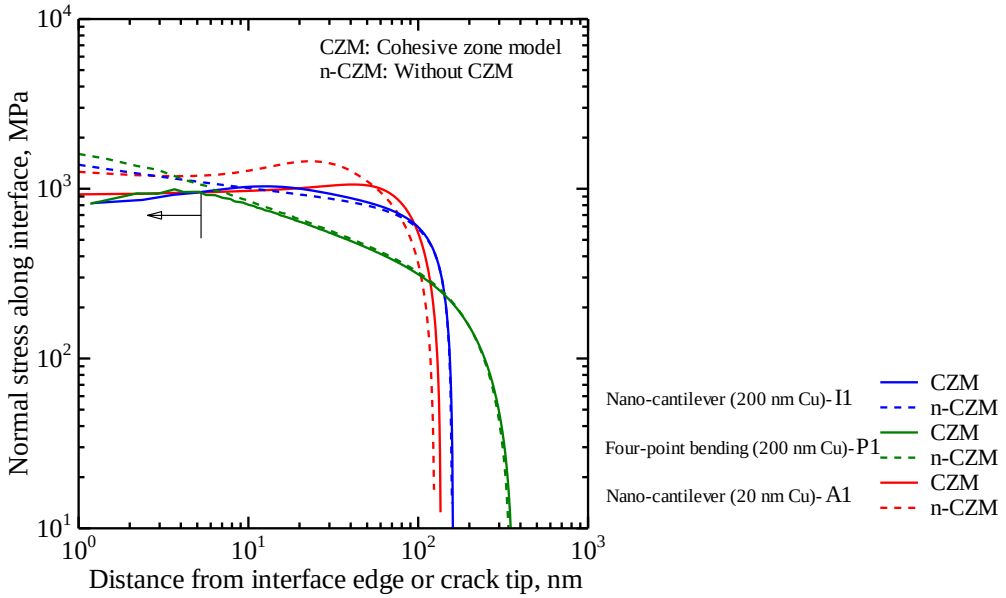

Fig. 11 Comparison of the stress distributions along the Cu/Si interface of different specimens with and without CZM

8. Conclusions

We have investigated the universal applicability of CZM to the initiation and the

propagation of interface cracking in nano-cantilever (20 nm and 200 nm Cu) tests and modified four-point bending (200 nm Cu) tests. The results obtained can be summarized as follows:

(1). By calibrating with the experimental results of the nano-cantilever (200 nm Cu) test, the CZM parameters of the Cu/Si interface were determined as follows: cohesive strength σ_{max} = 1060 MPa and interface characteristic length parameter δ_{max} = 1 nm.

(2). The obtained CZM parameters give excellent prediction of crack initiation at the Cu/Si interface edge in nano-cantilever (20 nm Cu) and (200 nm Cu) experiments regardless of the specimen geometry, plastic behavior and residual stress.

(3). The CZM predicts the crack propagation along the Cu/Si interface in the mm-sized modified four-point bending (200 nm Cu) specimen very well, though the specimen size has a difference of thousands of times. Moreover, this also shows the validity of the CZM parameters for prescribing the interface toughness under different stress singularities.

(4). The analysis on the stress distribution of the Cu/Si interface with CZM suggests that the fracture process zone is about 5 nm long, which is far smaller than the singular stress field in the 200 nm Cu specimens.

Acknowledgement

This work was supported by a Grant-in-Aid for Scientific Research (S) (Grant No. 21226005) of the Japan Society of the Promotion of Science (JSPS).

References

[1] Rice JR. Elastic fracture mechanics concepts for interfacial cracks. J Appl Mech 1988;55: 98–103.

[2] Hutchinson JW, Suo Z. Mixed mode cracking in layered materials. Adv Appl Mech 1992;29:63–191.

[3] Gradin PA. A fracture criterion for edge-bonded bimaterial bodies. J Compos Mater 1982;16:448–56.

[4] Reedy ED, Guess TR. Butt joint tensile strength: interface corner stress intensity factor prediction. J Adhesive Sci Technol 1995;9:237–51.

[5] Kitamura T, Shibutani T, Ueno T. Crack initiation at free edge of interface between thin films in advanced LSI. Eng Fract Mech 2002;69:1289–99.

[6] Kitamura T, Hirakata H, Itsuji T. Effect of residual stress on delamination from interface edge between nano-films. Eng Fract Mech 2003;70:2089–101.

[7] Shang F, Kitamura T, Hirakata H, Kanno I, Kotera H, Terada K. Experimental and theoretical investigations of delamination at free edge of interface between piezoelectric thin films on a substrate. Int J Solids Struct 2005;42(5-6):1729–41.

[8] Hirakata H, Takahashi Y, Truong DV, Kitamura T. Role of plasticity on interface crack initiation from a free edge and propagation in nano-component. Int J Fract 2007;145: 261–71.

[9] Sumigawa T, Shishido T, Murakami T, Kitamura T. Interface crack initiation due to nano-scale stress concentration. Mat Sci Eng A-Struct 2010;527:4796–803.

[10] Sumigawa T, Shishido T, Murakami T, Iwasaki T, Kitamura T. Evaluation on plastic deformation property of copper nano-film by nano-scale cantilever specimen. Thin solid films 2010;518:6040–7.

[11] Takahashi Y, Hirakata H, Kitamura T. Quantitative evaluation of plasticity of a ductile nano-component. Thin Solid Films 2007;516:1925–30.

[12] Charalambides PG, Lund J, Evans AG, McMeeking RM. A test specimen for determining the fracture resistance of bimaterial interfaces. J Appl Mech 1989;111:77–82.

[13] Ma Q. A four-point bending technique for studying subcritical crack growth in thin films and at interfaces. J Mater Res 1997;12(3):840–5.

[14] Dauskardt RH, Lane M, Ma Q, Krishna N. Adhesion and debonding of multi-layer thin film structures. Eng Fract Mech 1998;61:141–62.

[15] Hofinger I, Oechsner M, Bahr HA, Swain MV. Modified four-point bending specimen for determining the interface fracture energy for thin, brittle layers. Int J Fract 1998;92: 213–20.

[16] Rahulkumar P, Jagota A, Bennison SJ, Saigal S. Cohesive element modeling of viscoelastic fracture: application to peel testing of polymers. Int J Solids Struct 2000;37:1873–97.

[17] Siegmund T, Brocks W. A numerical study on the correlation between the work of separation and the dissipation rate in ductile fracture. Eng Fract Mech 2000;67:139–54.

[18] Camacho GT, Ortiz M. Computational modeling of impact damage in brittle materials. Int J Solids Struct 1996;33:2899–938.

[19] Foulk JW, Allen DH, Helms KLE. Formulation of a three-dimensional cohesive zone model for application to a finite element algorithm. Comput Methods Appl Mech Eng 2000;183:51–66.

[20] Barenblatt GI. Mathematical theory of equilibrium cracks in brittle fracture. Adv Appl Mech 1962;7:55–125.

[21] Dugdale DS. Yielding of steel sheets containing slits. J Mech Phys Solids 1960;8:100-4.

[22] Needleman A. A continuum model for void nucleation by inclusion debonding. J App Mech 1987;54:525–31.

[23] Needleman A. An analysis of tensile decohesion along an interface. J Mech Phys Solids 1990;38(3):289–324.

[24] Tvergaard V, Hutchinson JW. The relation between crack growth resistance and fracture process parameters in elastic-plastic solids. J Mech Phys Solids 1992;40(6):1377–97.

[25] Geubelle PH, Baylor J. Impact-induced delamination of laminated composites: a 2D simulation. Compos Part B-Eng 1998;29(5):589–602.

[26] Xu XP, Needleman A. Void nucleation by inclusion debonding in a crystal matrix. Model Simul Mater Sci 1993;1(2):111–32.

[27] Yan Y, Shang F. Cohesive zone modeling of interfacial delamination in PZT thin films. Int J Solids Struct 2009;46:2739–49.

[28] Truong DV, Kitamura T, Thanh VV. Crack initiation strength of an interface between a submicron-thick film and a substrate. Mater Design 2009;31(3):1450–6.

[29] Nix WD. Mechanical properties of thin films. Metall Mater Trans 1989;20:2217–45.

[30] Lee KS, Wuttiphan S, Hu XZ, Lee SK, Lawn BR. Contact-induced transverse fractures in brittle layers on soft substrates: a study on silicon nitride bilayers. J Am Ceram Soc 1998;81:571–80.

[31] Falk ML, Needleman A, Rice JR. A critical evaluation of cohesive zone models of dynamic fracture. J Phys IV 2001;11:43–52.

[32] Yuan H, Chen J. Computational analysis of thin coating layer failure using a cohesive zone model and gradient plasticity. Eng Fract Mech 2003;70:1929–42.

[33] Van den Bosch MJ, Schreurs PJG, Geers MGD. An improved description of the exponential Xu and Needleman cohesive zone law for mixed-mode decohesion. Eng Fract Mech 2006;73:1220–34.

[34] Xu X, Needleman A. Numerical simulations of fast growth in brittle solids. J Mech Phys Solids 1994;42:1397–434.

[35] Abdul-Baqi A, Van der Giessen E. Numerical analysis of indentation-induced cracking of brittle coatings on ductile substrates. Int J Solids Struct 2002;39:1427–42.